Title
Unique transmembrane domain interactions differentially modulate integrin αvβ3 and αIIbβ3 function

Journal
Proceedings of the National Academy of Sciences of the United States of America, 116(25)

ISSN
0027-8424

Authors
Litvinov, Rustem I
Mravic, Marco
Zhu, Hua
et al.

Publication Date
2019-06-18

DOI
10.1073/pnas.1904867116

Peer reviewed

Unique transmembrane domain interactions differentially modulate integrin αvβ3 and αIIbβ3 function

Rustem I. Litvinov[a,b,1], Marco Mravic[c,1], Hua Zhu[d], John W. Weisel[a], William F. DeGrado[c,e,2], and Joel S. Bennett[d,2]

[a]Department of Cell and Developmental Biology, University of Pennsylvania School of Medicine, Philadelphia, PA 19104; [b]Institute of Fundamental Medicine and Biology, Kazan Federal University, 420012 Kazan, Russian Federation; [c]Department of Pharmaceutical Chemistry, University of California, San Francisco, CA 94158; [d]Division of Hematology/Oncology, Department of Medicine, University of Pennsylvania School of Medicine, Philadelphia, PA 19104; and [e]Cardiovascular Research Institute, University of California, San Francisco, CA 94158

Contributed by William F. DeGrado, April 16, 2019 (sent for review March 21, 2019; reviewed by Renhao Li and Peter J. Newman)

Lateral transmembrane (TM) helix–helix interactions between single-span membrane proteins play an important role in the assembly and signaling of many cell-surface receptors. Often, these helices contain two highly conserved yet distinct interaction motifs, arranged such that the motifs cannot be engaged simultaneously. However, there is sparse experimental evidence that dual-engagement mechanisms play a role in biological signaling. Here, we investigate the function of the two conserved interaction motifs in the TM domain of the integrin β3-subunit. The first motif uses reciprocating "large-large-small" amino acid packing to mediate the interaction of the β3 and αIIb TM domains and maintain the inactive resting conformation of the platelet integrin αIIbβ3. The second motif, S-x_3-A-x_3-I, is a variant of the classical "G-x_3-G" motif. Using site-directed mutagenesis, optical trap-based force spectroscopy, and molecular modeling, we show that S-x_3-A-x_3-I does not engage αIIb but rather mediates the interaction of the β3 TM domain with the TM domain of the αv-subunit of the integrin αvβ3. Like αIIbβ3, αvβ3 on circulating platelets is inactive, and in the absence of platelet stimulation is unable to interact with components of the subendothelial matrix. However, disrupting any residue in the β3 S-x_3-A-x_3-I motif by site-directed mutations is sufficient to induce αvβ3 binding to the αvβ3 ligand osteopontin and to the monoclonal antibody WOW-1. Thus, the β3-integrin TM domain is able to engage in two mutually exclusive interactions that produce alternate α-subunit pairing, creating two integrins with distinct biological functions.

integrin activation | transmembrane domain | interaction motifs | force spectroscopy

Lateral transmembrane (TM) helix–helix interactions are central to the regulation of many proteins that transmit signals across membranes, including integrins (1). As a relevant example, a heterodimer composed by the TM helices of its αIIb- and β3-subunits stabilizes the integrin αIIbβ3 on circulating platelets in its resting inactive conformation, preventing the spontaneous formation of platelet aggregates in the circulation and ensuring that αIIbβ3 is only activated at sites of vascular injury (2). Molecular modeling has provided insight into the structure of the αIIbβ3 TM heterodimer (3). Initial models were built by combining rigid-body sampling and physics-based energy minimization subject to numerous restraints derived from biochemical experiments (4, 5). The resulting structural models were in remarkably good agreement with subsequent NMR structures of the TM domain heterodimer, highlighting the power of data-driven computer models of TM complexes in the absence of high-resolution structural information (6, 7).

The interface of the αIIbβ3 TM domain heterodimer consists of a tightly packed structure in which small and large residues interdigitate by efficient van der Waals packing along the heterodimer interface. Thus, a sequence motif in the αIIb TM domain, G-x_3-G-x_3-L, packs in a reciprocal manner with the β3 TM domain sequence V-x_3-I-x_3-G such that bulky residues from one TM helix contact a hole formed by a small Gly residue on the neighboring helix (8) (Fig. 1).

Platelets contain a second β3-integrin, αvβ3. Like αIIbβ3, αvβ3 on resting platelets is inactive until platelets are stimulated, after which it is able to bind to immobilized ligands such as the extravascular matrix proteins osteopontin (OPN) and vitronectin (9). Although αv and αIIb are homologous proteins, they share only 36.1% sequence identity (10). Nonetheless, compared with the αIIb TM domain motif interfacing with β3, the homologous motif on αv contains only one conservative Gly-to-Ala substitution (A-x_3-G-x_3-L) (8). On the other hand, most integrin β-subunits, including β3, also contain a highly conserved small residue-x_3-small residue motif (8) (Fig. 1 and *SI Appendix*, Table S1)—a motif in which the close interaction of small residues (Gly, Ala, and Ser) between two TM domains stabilizes dimeric TM complexes (11). However, the small residue-x_3-small residue motif S-x_3-A on the β3 TM helix is located on the face of the helix opposite the interface of the αIIbβ3 TM heterodimer (12) (Fig. 1).

Platelets circulate in a milieu containing a high concentration of the principal αIIbβ3 ligand fibrinogen (13). Thus, αIIbβ3 function is tightly regulated (14). Given the specialized nature of

Significance

Besides anchoring proteins in membranes, transmembrane (TM) helices facilitate the assembly of multisubunit proteins. Often, TM helices contain several TM–helix interaction sequences, arranged such that they cannot be simultaneously engaged. The TM helix of the β3-integrin subunit contains two different sequences that it uses to interact with two different α-subunits, one with αIIb and the other with αv. Because integrins have distinct biological functions, the ability of a single TM helix to use different sequences to interact with different partners likely contributes to this functional specificity. Thus, the ability to achieve binding on two faces of a single TM helix provides a mechanism to evolve new binding partners for integrins and likely other membrane proteins as well.

Author contributions: R.I.L., M.M., H.Z., J.W.W., W.F.D., and J.S.B. designed research; R.I.L., M.M., and H.Z. performed research; R.I.L., M.M., H.Z., J.W.W., W.F.D., and J.S.B. analyzed data; and R.I.L., M.M., W.F.D., and J.S.B. wrote the paper.

Reviewers: R.L., Emory University School of Medicine; and P.J.N., BloodCenter of Wisconsin.

The authors declare no conflict of interest.

[1]R.I.L. and M.M. contributed equally to this work.

[2]To whom correspondence may be addressed. Email: william.degrado@ucsf.edu or bennetts@pennmedicine.upenn.edu.

This article contains supporting information online at www.pnas.org/lookup/suppl/doi:10.1073/pnas.1904867116/-/DCSupplemental.

Published online June 3, 2019.

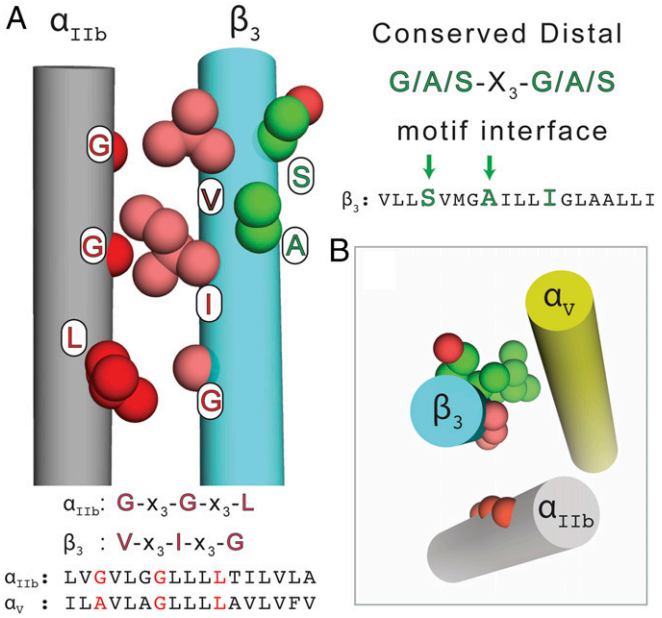

Fig. 1. Model of the αIIbβ3 TM domain heterodimer highlighting two conserved β3 interaction motifs. (*A*) The location of a conserved reciprocating large-small residue interfacial motif responsible for stabilizing the αIIbβ3 TM domain heterodimer is shown as red space-filling balls and its sequence is denoted by red text. The location of a conserved G-x_3-G–like motif is shown as green space-filling balls, and its sequence is denoted by green text and arrows. The presence of a conserved distal isoleucine residue is also denoted in the text. (*B*) Top-down view of the αIIbβ3-helices with only αIIbβ3 Cα-atoms shown. Also displayed is a potential interaction partner for the G-x_3-G–like motif, αv (yellow). Given the offset of their helical registers, the two β3 interaction motifs constitute two distinct interaction interfaces.

αIIbβ3 function, we asked whether the motifs mediating the interaction of the β3 TM domain with αv and αIIb are necessarily the same. To address this question, we scanned the TM helix of intact β3 with leucine and alanine replacements and used optical trap-based force spectroscopy to identify replacements that caused constitutive αvβ3 binding to immobilized OPN, a physiological αvβ3 ligand (15), and to the activation-dependent monovalent αvβ3-specific monoclonal antibody WOW-1 (16). In contrast to αIIbβ3, we found a clear shift in the helical register and periodicity of the αvβ3 TM heterodimer such that the αv- and β3-helices both interacted via small-x_3-small residue motifs. Subsequent unrestrained molecular dynamics simulations revealed that this helical interface was stable and in striking agreement with our functional results. Thus, the β3-integrin TM domain employs two distinct sequences that mediate mutually exclusive interactions producing alternate α-subunit pairing, creating two integrins with distinct biological functions.

Results

Effect of β3 TM Domain Mutations on OPN Binding to αvβ3. For integrin αIIbβ3, we previously showed that perturbing side-chain van der Waals packing at the TM domain interface shifts the protein from its resting inactive conformation to its active conformation, the latter having high ligand-binding affinity (17, 18). Scanning mutagenesis identified the β3 TM domain V-x_3-I-x_3-G motif responsible for stabilizing αIIbβ3 in its inactive state (19). Here, we interrogated the second platelet β3-integrin αvβ3 via mutagenesis of the β3 TM domain in conjunction with optical trap-based force spectroscopy to probe the activation state of the αvβ3 mutants (17, 20).

Optical trap-based force spectroscopy measurements of the binding of OPN-coated latex beads to CHO cells expressing wild-type (WT) αvβ3 are shown in Fig. 2. Data are expressed as the cumulative probability of detecting rupture forces >20 pN, normalized for the level of αvβ3 expression. The vast majority of the WT αvβ3 expressed on the CHO cell surface was in its resting state, with a cumulative probability of binding to OPN of 1.7 ± 0.8% (Fig. 2 *A* and *D*). Nonetheless, the small peak of rupture force at 55–70 pN indicated that a minor population of the WT αvβ3 was active and constitutively able to interact with OPN. We then repeated the measurements after adding 1 mM Mn^{2+} to the suspension medium to shift the equilibrium to favor the high-affinity αvβ3 conformation. There was a striking increase in the force spectrum with a peak in the range of 55–65 pN and with detectable rupture forces as large as 100 pN (Fig. 2*C*). Moreover, the cumulative probability of rupture forces >20 pN increased substantially to 9.1 ± 4.3%, significantly different ($P < 0.001$) compared with WT αvβ3 in the absence of Mn^{2+} (Fig. 2*D*). Lastly, because αvβ3 binding to ligands is dependent on the presence of divalent cations (21), we performed OPN binding in the presence of the chelator EDTA. The resulting force spectrum was nearly the same as that of WT αvβ3 in the absence of Mn^{2+}, with no statistical difference in the cumulative binding probability for forces >20 pN ($P > 0.05$). The vast majority of rupture forces are in the range of 0–40 pN, and the small peak in rupture force at 55–70 pN seen for WT is dissipated. These measurements indicate that the vast majority of the WT αvβ3 expressed on the surface of transfected CHO cells is in its resting inactive conformation, but that under appropriate conditions the inactive αvβ3 can be shifted to its active ligand-binding conformation.

We then tested the ability of specific alanine and leucine replacements in the β3 TM domain to cause constitutive αvβ3 activation. Critically, we found that replacing the first residue in the small residue-x_3-small residue motif in the β3 TM helix with a much bulkier leucine (S699L) caused strong constitutive αvβ3 activation. The rupture force spectrum for S699L is essentially

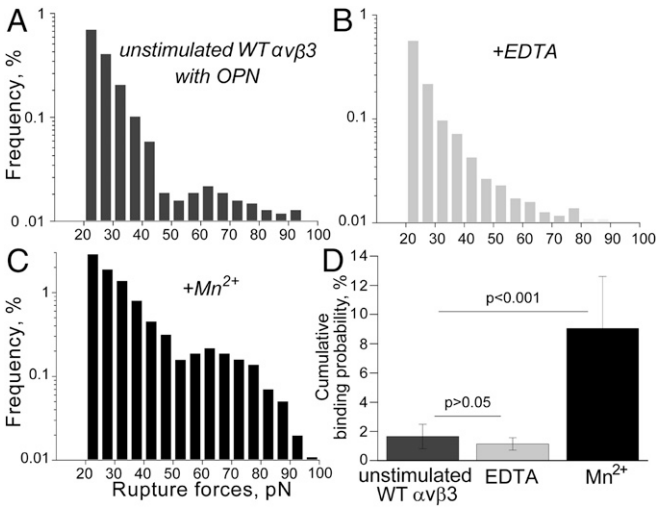

Fig. 2. Rupture force histograms of the interaction of OPN-coated latex beads with CHO cells expressing WT human αvβ3. Individual rupture force signals were collected into 5-pN bins and plotted as the percentage of total bead–cell contact–detachment cycles in a particular bin. Rupture forces of <20 pN representing background noise, optical artifacts, or nonspecific interactions were neglected. (*A*) Rupture force histograms resulting from OPN binding to unstimulated CHO cells expressing WT αvβ3. (*B*) Histograms in the presence of 5 mM EDTA. (*C*) Histograms in the presence of 1 mM Mn^{2+}. (*D*) Bar graph derived from the histograms shown in *A*–*C* indicating the cumulative probability of detecting rupture forces >20 pN. The statistical significance of differences in cumulative binding probability ± SEM was determined using the Mann–Whitney *U* test, with $P < 0.05$ considered to be statistically significant.

identical to that of WT αvβ3 fully activated by 1 mM Mn^{2+} (Fig. 2*C*). The range of rupture forces extended to 95 pN with a peak at 60–75 pN and a cumulative probability of rupture forces >20 pN of 9.9 ± 4.2% (Fig. 3 *A* and *D*). Addition of 1 mM Mn^{2+} to S699L induced only a modest increase in the cumulative binding probability for forces >20 pN, 11.3 ± 3.8%, while the addition of 5 mM EDTA caused substantial inhibition of rupture forces in the range of 30–55 pN and complete abrogation of those >55 pN (Fig. 3 *B*–*D*), consistent with the divalent cation dependence and specific binding between S699L αvβ3 and OPN.

The results of scanning the entire β3 TM domain with alanine or leucine replacements on αvβ3 binding to OPN are shown in Fig. 4*A* and *SI Appendix*, Table S2. They reveal that mutating either S699 or A703 that comprises the small residue-x_3-small residue motif in the β3 TM domain (^{699}S-x_3-A^{703}) causes constitutive OPN binding to αvβ3. By contrast, mutating the same residues did not cause constitutive fibrinogen binding to αIIbβ3 (19). To directly compare the TM domain interfaces of αvβ3 and αIIbβ3, we plotted the fractional activation of αvβ3 (OPN binding) versus the fractional activation of αIIbβ3 (fibrinogen binding) caused by mutating β3 TM domain residues 697–705 in Fig. 5*A*. The curves for constitutive αvβ3 and αIIbβ3 activation are completely out of phase, indicating that the residues critical for the interaction of αIIb versus αv with β3 reside on opposites sides of the β3-helix (Fig. 5*C*). Besides the high degree of αvβ3 activation caused by S699L and A703L, G702L and I707L are also highly activating. G702 is adjacent to A703, and I707 is one full α-helical turn down. Both of these residues lie on the same face of the α-helix as the ^{699}S-x_3-A^{703} motif (Fig. 4*A*). Thus, the β3 residues whose mutations cause constitutive αvβ3 activation (S699, G702, A703, I707) define a contiguous interaction interface on β3 with αv, with a different helical register and clearly distinct from the αIIbβ3 interface.

To confirm these results, we repeated the optical trap-based force spectroscopy measurements using the activation-dependent monovalent monoclonal antibody WOW-1 as a second αvβ3 ligand (16). As shown in Fig. 4*B* and *SI Appendix*, Table S2, force spectroscopy measurements using WOW-1 as the αvβ3 ligand were generally in agreement with those using OPN. As with OPN, large effects were seen for the S699L, A703L, and I707L mutants.

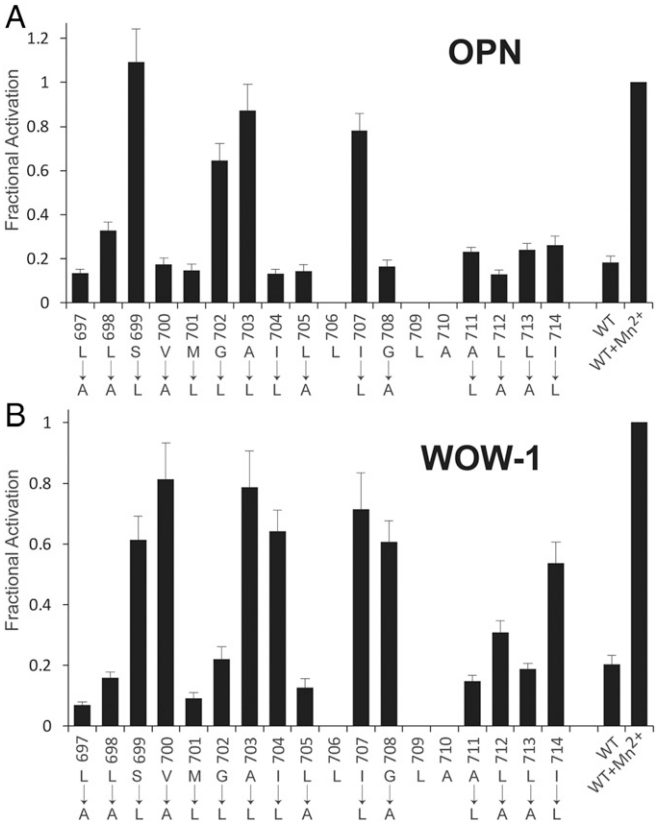

Fig. 4. Effects of leucine or alanine replacements in the β3 TM helix on the cumulative probability of constitutive OPN (*A*) and WOW-1 (*B*) binding to αvβ3 expressed by CHO cells. The β3 mutants were coexpressed with WT human αv in CHO cells, and the cumulative probabilities of constitutive OPN and WOW-1 binding to αvβ3 was measured by optical trap-based force spectroscopy. The cumulative probabilities of OPN and WOW-1 binding to WT αvβ3 in the absence and presence of 1 mM Mn^{2+} were used as negative and positive controls, respectively. The bars and error bars correspond to the mean and SE generated from rupture force histograms representing 10^4–10^5 bead–cell contacts in at least 10 independent experiments.

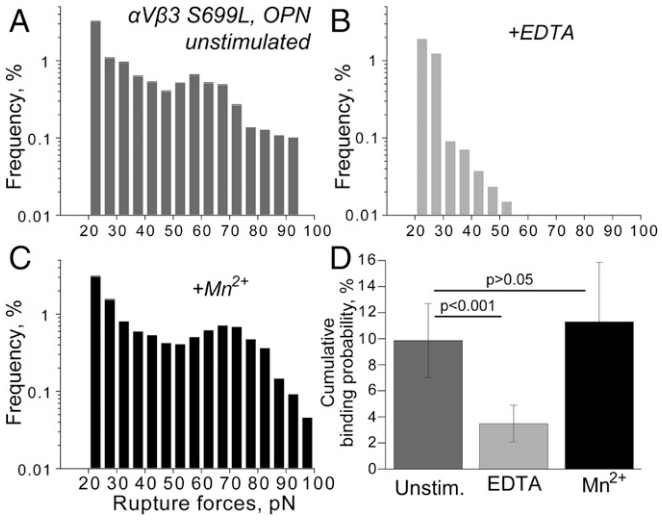

Fig. 3. Rupture force histograms of the interaction of OPN-coated latex beads with CHO cells expressing human αvβ3 containing the β3 TM helix mutation S699L. (*A*) Rupture force histograms resulting from OPN binding to unstimulated CHO cells expressing the β3 S699L αvβ3 mutant. (*B*) Histograms in the presence of 5 mM EDTA. (*C*) Histograms in the presence of 1 mM Mn^{2+}. (*D*) Bar graph derived from the histograms shown in *A*–*C* indicating the cumulative probability ± SEM of detecting rupture forces >20 pN. Unstim., unstimulated αVβ3 S699L.

Moreover, the subtle isomeric replacement of Ile707 with Leu resulted in αvβ3 activation, demonstrating that the native van der Waals packing interactions are highly stereochemically specific. It is noteworthy that mutating residues V700, I704, and G708 that neighbor S699, A703, and I707 was more activating when WOW-1 binding was measured compared with OPN binding. This might reflect a higher affinity of WOW-1 for αvβ3 such that marginally activated mutants were detected more easily. By contrast, replacing G702 with leucine was less activating when WOW-1 was the αvβ3 ligand. Likewise, it is also possible that WOW-1 binds to a different range of activated αvβ3 conformations from the physiological αvβ3 ligand OPN. Despite these differences, the overall trend is similar between mutants binding to OPN and WOW-1. These results confirm that the conserved β3 S-x_3-A-x_3-I motif is critical for gating αvβ3 activation, and that the TM domain surface on β3 used to bind αv is quite distinct from that used in αIIbβ3.

Modeling and Molecular Dynamics Simulation of αvβ3. To gain a better structural understanding of the αvβ3 TM domain interface, we compared the helical register implied from our scanning mutagenesis of αvβ3 to the interfaces calculated for two independently published solution NMR structures of aIIbβ3 (6, 7). First, we analyzed the per-residue interhelical distances between each residue in β3 and the closest residues in αIIb by Cα-atom for the lowest-energy model reported in each NMR study.

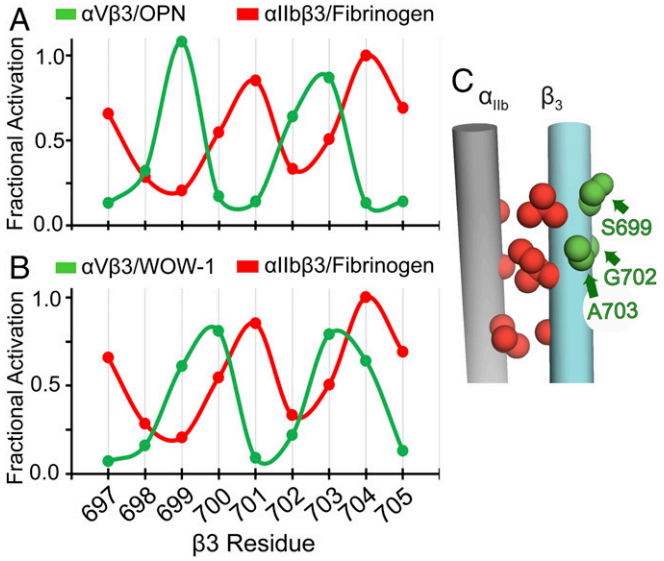

Fig. 5. Motifs in the β3 TM helix that mediate its association with αv and αIIb are completely out of phase and are located on opposites sides of the β3-helix. (*A*) The curves compare the effect of replacing β3 residues 697–705 with leucine or alanine on constitutive αvβ3 binding to OPN using data from Fig. 4*A* and the effect of the same replacements on constitutive αIIbβ3 to fibrinogen using data from ref. 4. (*B*) The curves compare the effect of replacing β3 residues 697–705 on constitutive αvβ3 binding to WOW-1 using data from Fig. 4*B* and the effect of these replacements on constitutive αIIbβ3 to fibrinogen using data from ref. 4. (*C*) The β3 residues whose mutation causes constitutive binding of αvβ3 to OPN (S699, G702, and A703) are shown as green spheres on the αIIbβ3 TM structure cylinders. This demonstrates that the residues responsible for the interaction of β3 with αIIb versus αv reside on opposites sides of the β3-helix.

To make comparisons to the per-residue change associated with αvβ3 mutant binding to OPN, the interhelical distances were converted to a normalized interhelical closeness (NIC) value, as described in *SI Appendix*, *Materials and Methods*, where NIC = 1 for the closest β3 residue to the αIIb backbone and NIC = 0 for the farthest β3 residue (*SI Appendix*, Fig. S1*A*). When the NIC values for the two αIIbβ3 NMR structures are plotted alongside the fractional activation values for αvβ3 binding to OPN shown in Fig. 4, it is clear that mutating residues in the β3 TM helix that are closest to the αIIb-helix would have no effect on the activation state of avβ3 (*SI Appendix*, Fig. S1*B*). Further, this analysis indicates that any attempt to model the avβ3 TM dimer from an αIIbβ3 NMR structure would require large-scale conformational rearrangements.

Next, we sought to build a model for all-atom molecular dynamics simulations to sample the energetic landscape of the αvβ3 TM and cytoplasmic domains. An initial model was built by threading the sequences of αv and β3 onto the coordinates of the first conformation of the reported αIIbβ3 NMR model (PDB ID code 2knc). This model was first structurally relaxed in an implicit lipid bilayer using the Rosetta modeling suite, applying rounds of side-chain rotamer sampling, cartesian minimization, and rigid-body reorientation. The resultant lowest-energy model was inserted into a POPC lipid bilayer, solvated, and equilibrated with constraints on the initial Cα-atomic positions. Constraints were then released for 400 ns of unbiased simulation time. Thereafter, each frame was structurally clustered using a 2.6-Å cutoff to identify unique conformations. Additionally, for each simulation frame, a Pearson correlation was calculated between the per-residue interhelical distances across the αvβ3 TM domain (i.e., NIC of β3 residues) and the per-residue fractional activation datasets for both OPN and WOW-1 binding (Fig. 6*A*).

Within the first 20 ns of unrestrained simulation, the αv and β3 TM helices rapidly reoriented to a new geometry (Movies S1 and S2) with S699, A703, and I707 at the interface, resulting in a marked increase in the correlation between the model and the scanning mutagenesis results (Fig. 6 *A* and *B*). After remaining in this associated state for 75 ns, the TM helices dissociated in a conformation that persisted for an additional 70 ns. Meanwhile, the cytoplasmic domains remained in contact, including the αv R995–β3 E723 salt bridge (*SI Appendix*, Fig. S2). The αvβ3 TM heterodimer was reconstituted with an interhelical geometry similar to that before dissociation, persisting in this conformation for the remaining 245 ns.

The major TM domain conformation (cluster medoid, 80.4% of 400 ns) had a consistently low structural deviation within the cluster (mean Cα rmsd = 1.20 ± 0.01, SEM) suggesting that it is energetically stable. Further, there was a statistically significant correlation between frames in this cluster and the rupture force spectroscopy results ($P < 0.05$). An overlay of the rupture force spectroscopy results for each β3 mutation and the interhelical distance for each β3 residue in the αvβ3 TM domain, as measured from a representative model of the major conformation, is shown in Fig. 6*B*. It is noteworthy that the modeled interface agrees well with both datasets. Further, while the average correlation with simulation frames is greater for the WOW-1 data than for the OPN data, the change in correlation coefficient between the initial and the medoid frames is greater for the OPN data than for the WOW-1 data.

A representative simulation snapshot depicting the αvβ3 TM dimer interface is shown in Fig. 6*C*. The helices adopt a geometry that is similar to the canonical GAS_{Right} motif (1) in its parallel right-handed crossing (−23.9 ± 0.3°, SEM), but differs in its larger interhelical distance of 10.2 ± 0.1 Å. We find αv side chains packing against the β3 residues most sensitive to mutation. Overall, the agreement of the major conformation from the simulation with the rupture force spectroscopy results is remarkable, given that no additional forces were applied to the system to bias helix association or geometry.

Discussion

TM domain interactions, mediated by specific sequence motifs, stabilize integrins in their inactive conformations (2, 22, 23). In the best characterized example, a canonical G-x_3-G motif in the αIIb TM helix packs against a reciprocating large residue-small residue motif in the β3 TM helix to stabilize the integrin αIIbβ3 in its inactive state (Fig. 1). Given the high degree of sequence conservation in both α- and β-chains, it seemed likely that this TM domain complex might be common to all integrins. This notion was supported by our previous measurements of heterodimeric interaction strength between the TM domain segments of integrins in *Escherichia coli* using the dominant-negative TOXCAT assay (8). In striking contrast, the results presented here using the full-length protein in mammalian membranes indicate that the second platelet integrin αvβ3 is instead regulated by a distinct TM domain interface, which is also highly conserved (*SI Appendix*, Table S1).

When expressed in bacterial cell membranes, the β3 residues most sensitive to mutations were residues at the αIIbβ3 interface (8). Thus, the geometry of the isolated αvβ3 TM domain heterodimer assembled in bacterial membranes appears to differ from the geometry of the TM domain heterodimer when it is present in the context of the full-length receptor and expressed in mammalian membranes. This suggests that either the lipid environment or contiguous extracellular or intracellular sequences influence the conformation of the αv TM domain (24, 25).

Crystal structures of the αvβ3 and αIIbβ3 ectodomains and negatively stained electron microscopy images of the full-length proteins are similar (26–29). However, in the more membrane-distal regions of the β3 ectodomain, the interactions with either

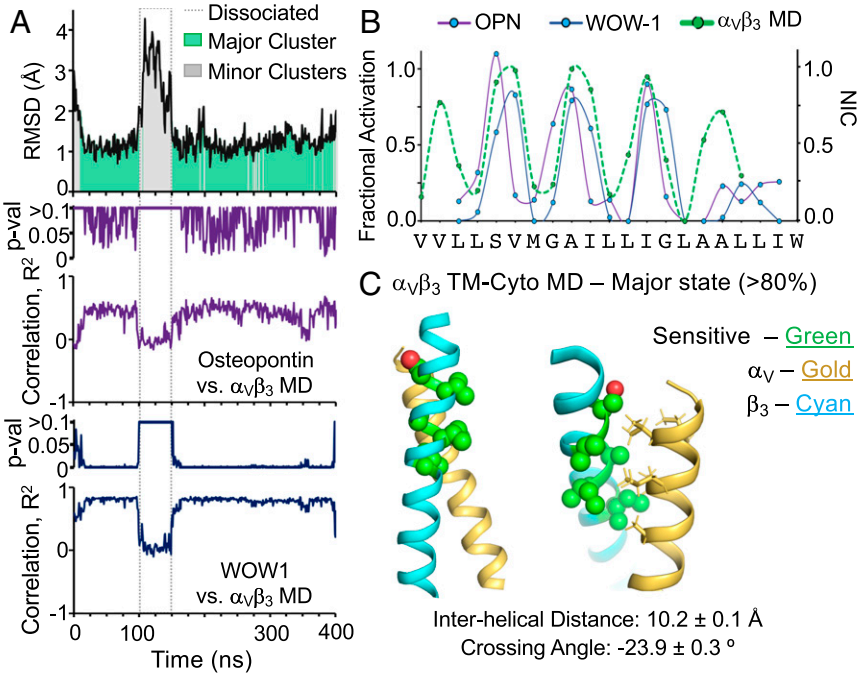

Fig. 6. Molecular dynamics simulations of αvβ3 TM and cytoplasmic domain interactions during αvβ3 binding to OPN and WOW-1. (*A*, *Upper*) Rmsd of the αvβ3 TM domain to the centroid of the major structural cluster. The color of each frame indicates whether it belongs to the major cluster (green) or a minor cluster (gray). (*A*, *Middle* and *Bottom*) Pearson correlation coefficients and *P* values of αvβ3 TM domain interhelical distances for each β3 mutation and the cumulative probability of OPN (*Middle*) or WOW-1 (*Bottom*) binding. (*B*) Overlay of the normalized interhelical distance values (interhelical closeness) for the major αvβ3 TM domain conformation observed in the MD simulations and the fractional activation of αvβ3 caused by β3 TM helix mutations using the results shown in Fig. 4. (*C*) Representative model of the major conformation and the mean geometric parameters ± SEM of the αvβ3 TM domain heterodimer observed during the MD simulations.

αv or αIIb that help maintain the inactive conformations of αvβ3 and αIIbβ3 differ (25). Consequently, the orientation of the distal β3-stalk and the contiguous β3 TM helix might be expected to be shifted with respect to complementary portions of αv and αIIb as well. While the composition of the αIIbβ3 TM domain interface heterodimer is well-established, there has been until now a paucity of information about the structure of the αvβ3 TM domain. Although the αIIb and αv TM domains each contain a small residue-x_3-small residue motif in approximately the same position, their van der Waal surfaces are certainly distinct and distinguishable, since computationally designed TM domain peptides were able to interact exclusively with either αv or αIIb (30). Then, it is not surprising that β3 can interact with αv and αIIb via distinct interfaces, varying in affinity (17, 31).

The distinct TM domain interface between αvβ3 and αIIbβ3 might be rationalized by their varying requirements for stringent regulation of the high-affinity ligand-binding conformation given their different physiological roles. αvβ3 is widely expressed, mediating cell adhesion and migration on a variety of immobilized ligands containing an RGD motif (32), while αIIbβ3 expression is limited to platelets. Moreover, αIIbβ3 readily interacts with soluble ligands, whereas αvβ3 does not. Previously, using optical trap-based force spectroscopy, we found that under essentially identical conditions, the average adhesion strength for OPN–αvβ3 interactions was 47 ± 7 pN, whereas the average adhesion strength of fibrinogen binding to αIIbβ3 was nearly twofold greater at 80–90 pN (20, 33). This may be a reflection of the physiological requirement that fibrinogen binding to αIIbβ3 on aggregated platelets must be sufficiently strong to resist the shear forces present in arterial blood, which would not be the case for the adherence and spreading of single platelets mediated by ligand binding to αvβ3. Further, we found that a substantial fraction of unstimulated platelets exhibit a distribution of OPN-mediated rupture forces similar to ADP-stimulated platelets (20), whereas the fraction of unstimulated platelets that interact spontaneously with fibrinogen is negligible (33). This implies that αIIbβ3 is less prone to activation than αvβ3, perhaps a consequence of the differences in the interfaces of their TM domains.

From a biophysical perspective, the structural consequences of the mutations observed here are consistent with the literature but also offer new insights. Employing small-to-large or large-to-small mutations successfully induced major disruptions in van der Waals packing at the TM heterodimer interface. However, deviation of this pattern to much more subtle mutants, namely Leu-Ile or Ile-Leu isomers, also had dramatic effects. For example, Ile707Leu had a marked effect on both OPN and WOW-1 binding, despite only one methyl group being stereochemically repositioned in the entire protein complex. This indicates a strict steric requirement for van der Waals packing interactions between TM domain side chains that dictates the stability and regulation of the αvβ3 resting state. Similar Ile-Leu mutations have been observed to abrogate select TM domain interactions for shorter engineered TM peptides (34, 35), yet it is noteworthy to find a similar result within a large protein complex interacting simultaneously through several extramembrane domains. The mutational consequences might also be rationalized in the context of previous reports for small-x_3-small motifs. Replacement of the neighboring β-branched residues V700 and I704 with alanine and leucine, respectively, caused constitutive WOW-1 binding to αvβ3 as well. In a statistical analysis of amino acid patterns in TM helices, Senes et al. (11) found that not only were small-x_3-small residue motifs frequent but these motifs were commonly associated with β-branched aliphatic residues in neighboring $i \pm 1$ positions. Further, they posited that because the side chains of valine and isoleucine are constrained to only one rotamer when they are present in a helix, these residues contribute to the stability of transmembrane helix dimers by minimizing entropy loss upon helical packing. Thus, it is possible that by mutating either V700 to alanine or I704 to leucine, the αvβ3 TM domain is destabilized sufficiently to permit WOW-1 binding to a different range of activated αvβ3 conformations but not the more stringent binding of OPN.

Our MD simulations are also consistent with numerous experimentally reported features of the αvβ3 cytosolic and juxtamembrane regions (24, 36). The homology model began with the entire cytoplasmic domains of both αv and β3 as α-helical, yet we observed that only αv V993–V1024 and β3 D718–N769 had persistent α-helical structure with the remaining regions in extended conformations. This is consistent with NMR measurements of a β3 TM–cytoplasmic construct in DHPC:DMPC bicelles where

β3 was helical through residue A737, well beyond the TM domain and into the cytoplasm (24). Also consistent with this NMR study, K713 (numbered K716 in ref. 24) snorkeled its amine moiety to the cytoplasmic lipid head-group region in the majority of simulations. We also found that the R995-to-E723 salt bridge previously suggested to stabilize the low-affinity state of αvβ3 (36) formed during the initial structural relaxation of the αvβ3 homology model and was maintained through the first 260 ns of simulation, even during the TM helix dissociation event (*SI Appendix*, Fig. S2). Nonetheless, in the last 60 ns, we observed a switch to a K994–E723 salt bridge. Although the simulation does not completely sample the orientational and conformational energy landscapes available to αvβ3, in this short timescale, we observed behavior largely consistent with previous structural and functional experiments of αvβ3, implying that the simulated conformation may be physiologically relevant. Thus, the MD simulations are consistent with a unique interface for the αvβ3 TM heterodimer. Our final model, derived entirely from unbiased simulations, shown in Fig. 6*C*, provides atomic-level understanding of the TM domain interactions that constrain αvβ3 in its inactive state, as well as insight into how homologous integrins uniquely regulate cellular signal transduction.

Conclusion

TM helix–helix interactions are known to play important roles in the function of many type 1 membrane proteins, including integrins and receptor-linked tyrosine kinases. Often the TM helices contain two TM–helix interaction motifs, arranged such that both motifs cannot simultaneously engage a single target without large structural distortions. At the outset of our investigation, we expected that the different helix–helix interaction motifs might be alternatively engaged during the dynamics of signaling, as has been proposed for members of the EGF receptor family (37, 38). Therefore, we were surprised to find that the two motifs found in the β3 TM helix mediate interactions with two different α-subunits. Given the combinatorial assembly of integrin subunits into heterodimers with distinct biological functions, the ability of a single TM domain to use two different faces of its helix for different interaction partners is noteworthy. This phenomenon might contribute to both the specificity of interaction and the different activation energies required for different receptors. Moreover, the ability to achieve binding on two faces of a single helix provides an attractive mechanism to evolve new partners in the integrin family as well as other membrane proteins.

Materials and Methods

DNA cloning, cell culture, and force spectrometry materials were obtained from commercial sources and used as described in *SI Appendix*. Molecular modeling and dynamics simulations were conducted using publicly available software and analyzed as described in *SI Appendix*.

ACKNOWLEDGMENTS. This work was supported by NIH Grants R35GM122603 (to W.F.D.) and HL40387 (to J.S.B., J.W.W., and W.F.D.). M.M. is supported by an HHMI Gilliam Fellowship and a UCSF Discovery Fellowship. R.I.L. acknowledges the Program for Competitive Growth at Kazan Federal University.

1. R. F. Walters, W. F. DeGrado, Helix-packing motifs in membrane proteins. *Proc. Natl. Acad. Sci. U.S.A.* **103**, 13658–13663 (2006).
2. R. Li *et al*., Activation of integrin alphaIIbbeta3 by modulation of transmembrane helix associations. *Science* **300**, 795–798 (2003).
3. K. E. Gottschalk, P. D. Adams, A. T. Brunger, H. Kessler, Transmembrane signal transduction of the alpha(IIb)beta(3) integrin. *Protein Sci.* **11**, 1800–1812 (2002).
4. J. Zhu *et al*., The structure of a receptor with two associating transmembrane domains on the cell surface: Integrin alphaIIbbeta3. *Mol. Cell* **34**, 234–249 (2009).
5. D. G. Metcalf, D. W. Kulp, J. S. Bennett, W. F. DeGrado, Multiple approaches converge on the structure of the integrin alphaIIb/beta3 transmembrane heterodimer. *J. Mol. Biol.* **392**, 1087–1101 (2009).
6. J. Yang *et al*., Structure of an integrin alphaIIb beta3 transmembrane-cytoplasmic heterocomplex provides insight into integrin activation. *Proc. Natl. Acad. Sci. U.S.A.* **106**, 17729–17734 (2009).
7. T. L. Lau, C. Kim, M. H. Ginsberg, T. S. Ulmer, The structure of the integrin alphaIIbbeta3 transmembrane complex explains integrin transmembrane signalling. *EMBO J.* **28**, 1351–1361 (2009).
8. B. W. Berger *et al*., Consensus motif for integrin transmembrane helix association. *Proc. Natl. Acad. Sci. U.S.A.* **107**, 703–708 (2010).
9. J. S. Bennett, C. Chan, G. Vilaire, S. A. Mousa, W. F. DeGrado, Agonist-activated alphavbeta3 on platelets and lymphocytes binds to the matrix protein osteopontin. *J. Biol. Chem.* **272**, 8137–8140 (1997).
10. L. A. Fitzgerald *et al*., Comparison of cDNA-derived protein sequences of the human fibronectin and vitronectin receptor alpha-subunits and platelet glycoprotein IIb. *Biochemistry* **26**, 8158–8165 (1987).
11. A. Senes, M. Gerstein, D. M. Engelman, Statistical analysis of amino acid patterns in transmembrane helices: The GxxxG motif occurs frequently and in association with beta-branched residues at neighboring positions. *J. Mol. Biol.* **296**, 921–936 (2000).
12. M. Hoefling, H. Kessler, K. E. Gottschalk, The transmembrane structure of integrin alphaIIbbeta3: Significance for signal transduction. *Angew. Chem. Int. Ed. Engl.* **48**, 6590–6593 (2009).
13. J. S. Bennett, Platelet-fibrinogen interactions. *Ann. N. Y. Acad. Sci.* **936**, 340–354 (2001).
14. J. S. Bennett, Structure and function of the platelet integrin alphaIIbbeta3. *J. Clin. Invest.* **115**, 3363–3369 (2005).
15. C. M. Giachelli, L. Liaw, C. E. Murry, S. M. Schwartz, M. Almeida, Osteopontin expression in cardiovascular diseases. *Ann. N. Y. Acad. Sci.* **760**, 109–126 (1995).
16. N. Pampori *et al*., Mechanisms and consequences of affinity modulation of integrin alpha(V)beta(3) detected with a novel patch-engineered monovalent ligand. *J. Biol. Chem.* **274**, 21609–21616 (1999).
17. R. I. Litvinov *et al*., Activation of individual alphaIIbbeta3 integrin molecules by disruption of transmembrane domain interactions in the absence of clustering. *Biochemistry* **45**, 4957–4964 (2006).
18. W. Li *et al*., A push-pull mechanism for regulating integrin function. *Proc. Natl. Acad. Sci. U.S.A.* **102**, 1424–1429 (2005).
19. H. Zhu *et al*., Specificity for homooligomer versus heterooligomer formation in integrin transmembrane helices. *J. Mol. Biol.* **401**, 882–891 (2010).
20. R. I. Litvinov, G. Vilaire, H. Shuman, J. S. Bennett, J. W. Weisel, Quantitative analysis of platelet alpha v beta 3 binding to osteopontin using laser tweezers. *J. Biol. Chem.* **278**, 51285–51290 (2003).
21. O. Helluin *et al*., The activation state of alphavbeta 3 regulates platelet and lymphocyte adhesion to intact and thrombin-cleaved osteopontin. *J. Biol. Chem.* **275**, 18337–18343 (2000).
22. B. H. Luo, T. A. Springer, J. Takagi, A specific interface between integrin transmembrane helices and affinity for ligand. *PLoS Biol.* **2**, e153 (2004).
23. D. T. Moore, B. W. Berger, W. F. DeGrado, Protein-protein interactions in the membrane: Sequence, structural, and biological motifs. *Structure* **16**, 991–1001 (2008).
24. Z. Lu *et al*., Implications of the differing roles of the β1 and β3 transmembrane and cytoplasmic domains for integrin function. *eLife* **5**, e18633 (2016).
25. J. E. Donald, H. Zhu, R. I. Litvinov, W. F. DeGrado, J. S. Bennett, Identification of interacting hot spots in the beta3 integrin stalk using comprehensive interface design. *J. Biol. Chem.* **285**, 38658–38665 (2010).
26. J. P. Xiong *et al*., Crystal structure of the extracellular segment of integrin alpha Vbeta3. *Science* **294**, 339–345 (2001).
27. B. D. Adair *et al*., Three-dimensional EM structure of the ectodomain of integrin alphaVbeta3 in a complex with fibronectin. *J. Cell Biol.* **168**, 1109–1118 (2005).
28. J. Zhu *et al*., Structure of a complete integrin ectodomain in a physiologic resting state and activation and deactivation by applied forces. *Mol. Cell* **32**, 849–861 (2008).
29. E. T. Eng, B. J. Smagghe, T. Walz, T. A. Springer, Intact alphaIIbbeta3 integrin is extended after activation as measured by solution X-ray scattering and electron microscopy. *J. Biol. Chem.* **286**, 35218–35226 (2011).
30. H. Yin *et al*., Computational design of peptides that target transmembrane helices. *Science* **315**, 1817–1822 (2007).
31. G. Pagani, H. Gohlke, On the contributing role of the transmembrane domain for subunit-specific sensitivity of integrin activation. *Sci. Rep.* **8**, 5733 (2018).
32. R. O. Hynes, Integrins: Bidirectional, allosteric signaling machines. *Cell* **110**, 673–687 (2002).
33. R. I. Litvinov, D. H. Farrell, J. W. Weisel, J. S. Bennett, The platelet integrin αIIbβ3 differentially interacts with fibrin versus fibrinogen. *J. Biol. Chem.* **291**, 7858–7867 (2016).
34. L. He *et al*., Single methyl groups can act as toggle switches to specify transmembrane protein-protein interactions. *eLife* **6**, e27701 (2017).
35. M. Mravic *et al*., Packing of apolar side chains enables accurate design of highly stable membrane proteins. *Science* **363**, 1418–1423 (2019).
36. M. A. Müller *et al*., Cytoplasmic salt bridge formation in integrin αvß3 stabilizes its inactive state affecting integrin-mediated cell biological effects. *Cell. Signal.* **26**, 2493–2503 (2014).
37. M. Lelimousin, V. Limongelli, M. S. Sansom, Conformational changes in the epidermal growth factor receptor: Role of the transmembrane domain investigated by coarse-grained metadynamics free energy calculations. *J. Am. Chem. Soc.* **138**, 10611–10622 (2016).
38. J. K. L. Sinclair, A. S. Walker, A. E. Doerner, A. Schepartz, Mechanism of allosteric coupling into and through the plasma membrane by EGFR. *Cell Chem Biol* **25**, 857–870.e7 (2018).